



Contents lists available at ScienceDirect

Electrochimica Acta

journal homepage: www.elsevier.com/locate/electacta



Electrochemistry on binary valve metal combinatorial libraries: niobium-tantalum thin films

Andrei Ionut Mardare^{a,*}, Alfred Ludwig^b, Alan Savan^b, Achim Walter Hassel^{a,c}

^a Institute for chemical technology of inorganic materials Johannes Kepler University Linz, 4040, Linz, Austria

^b Institut für Werkstoffe Ruhr-Universität Bochum 44780 Bochum, Germany

^c Christian Doppler Laboratory for combinatorial oxide chemistry at the institute for chemical technology of inorganic materials, Johannes Kepler University Linz, 4040, Linz, Austria

ARTICLE INFO

Article history:

Received 25 December 2013

Received in revised form 24 February 2014

Accepted 24 February 2014

Available online xxx

Keywords:

Combinatorial libraries

High-throughput experimentation

Scanning droplet cell microscopy

Anodic oxide films

ABSTRACT

A Nb-Ta thin film compositional spread obtained from a co-sputtering process was analysed. The microstructure and crystallographic investigations revealed the presence of a compositional threshold at Nb-60 at.%Ta where the change from tetragonal to cubic symmetry was evidenced by a mixed tetragonal-cubic phase. The electrochemical properties of the anodic oxides were studied via cyclic voltammetry and the oxide formation factors were mapped along the entire compositional spread. Values ranging from $1.8 \text{ nm} \cdot \text{V}^{-1}$ at the Ta-rich side to $2.6 \text{ nm} \cdot \text{V}^{-1}$ at the Nb-rich side of the library were measured. All Nb-Ta mixed anodic oxides were found to exhibit a type-n semiconducting behaviour as evidenced by Mott-Schottky analysis. The chemical composition of the surface anodic oxides differed from the composition of the parent metal alloys and no clear trend could be identified regarding their mismatch.

© 2014 Elsevier Ltd. All rights reserved.

1. Introduction

Tantalum being named after Tantalus and niobium after his daughter Niobe (both from Greek mythology) are typical valve metals exhibiting extremely stable oxides. According to the Pourbaix diagrams they show an extremely large range of stability, e.g. for tantalum a region of relative predominance of the oxide ranges from pH -2 to pH 16 [1]. These oxides are so stable that Ta was thought to be a noble metal until the mid of last century and it was listed as such [2]. These elements are chemically very similar as they are both from the 5th group and ⁷³Ta is heavily influenced by the lanthanoids contraction resulting in an identical atomic radius of 145 pm. Logically, they are often found in identical minerals able to replace each other.

The high dielectric properties make tantalum oxide the prime choice for high performance electrolytic capacitors which can have a breakdown field strength as high as the oxide formation field strength [3]. Addition of W to Ta thin films was recently proven to enhance the capacitance of barrier-type anodic films at low formation potentials [4]. The presence of Ta in various alloys in both bulk and thin films leads toward improved chemical stabilities. Excellent corrosion resistance was recently proven when Ti was alloyed with

Ta either by atmospheric high-velocity electron beam cladding of powder materials [5] or by plasma tantalumising in vacuum [6]. The more abundant Nb is cheaper than Ta and therefore a lot of research activities are dedicated to the replacement of Ta or the use of Nb-Ta alloys. Very interesting dielectric properties have been found in bulk Ag perovskite structures containing almost equal amounts of Ta and Nb with applications as high permittivity microwave ceramics [7]. Thick and thin films of Ag perovskite functional materials containing Ta and Nb were reported to have very good electrical properties with low dielectric losses, high permittivities with small frequency dependence and low leakage currents [8]. Ta and Nb additions have been shown to increase the high temperature strength of Pt-based alloys [9] which is of particular interest when such thin film is used as a heating element [10]. Both elements can be added as an alloying element and later during use at higher temperatures in an oxygen containing atmosphere they will be oxidised to form small oxide particles within the platinum. This process is called oxide dispersion strengthening since these small particles hinder direct sliding of crystallographic planes. In combination with Ni, Ta and Nb alloys can form bulk metallic glasses which due to their amorphous structure have shown high fracture strength, high corrosion resistance and high thermal stability [11,12].

Both Nb and Ta belong to the valve metal family (typically represented by Al) which produce barrier-type anodic oxides, usually amorphous, at high current efficiencies. Apart from the bulk applications mentioned before, these metals are also highly interesting

* Corresponding author. Tel.: +4373224688702; fax: +43 732 2468 8905.
E-mail address: andrei.mardare@jku.at (A.I. Mardare).

in their thin film form. Recent applications of anodic oxides on valve metal thin films include plastic electronics, when a polymeric flexible substrate is used for fabrication of MIM or MOS-FET structures, thus opening new directions in modern electronics [13]. Studying the mixed Nb-Ta anodic oxide properties is highly relevant especially due to their high dielectric constants, high breakdown fields and interesting photoelectrochemical behaviour under UV irradiation [14]. Recently, field crystallization of anodic oxides grown on Nb-Ta thin film alloys revealed an almost linear dependence between the alloy composition and oxide properties, i.e. oxide formation factor, density and permittivity [15].

High throughput combinatorial methods for recent material properties screening became largely used techniques in latest years. Recent research directions including battery development, electrocatalysis, photocatalysis, corrosion protection, sensor development, photovoltaics and light-emitting materials, etc. are dependent on combinatorial electrochemistry [16–18]. In the current work, a high throughput study of localized anodic oxidation of a wide compositional spread Nb-Ta thin film combinatorial library using a scanning droplet cell microscope is presented.

2. Experimental

2.1. Preparation of Nb-Ta compositional spread

Nb-Ta gradient composition thin films were obtained using co-sputtering in an ultra-high vacuum system (DCA, Finland) using two sputtering targets, 101.6 mm in diameter. Both targets were pure-element sputtering targets (99.995%, Kaistar R&D) and were placed at an angle of 144° to one another while aimed at the centre of the substrates. Both Ta and Nb were sputtered in the RF mode using a power of 200 W which resulted in deposition rates of $0.73 \text{ nm}\cdot\text{s}^{-1}$ and $0.49 \text{ nm}\cdot\text{s}^{-1}$, respectively. Three thermally oxidised Si wafers with an oxide thickness of approximately $1 \mu\text{m}$ and with diameters of 100 mm were sequentially used as substrates for the combinatorial deposition. Using this co-sputtering method, due to the vapour phase mixing of both sputtered species an overall compositional spread ranging from Nb-5 at.%Ta to Nb-94 at.%Ta was achieved defining the Nb-Ta thin film library. This spread translates into a compositional resolution of $0.3 \text{ at.}\% \text{ mm}^{-1}$. For all depositions, the base pressure of the vacuum chamber was in the range of $2\cdot 10^{-6} \text{ Pa}$. The samples were deposited at room temperature in Ar atmosphere with a pressure of $6\cdot 10^{-1} \text{ Pa}$. The distances between targets and substrate were kept constant at 190 mm, which resulted in total film thicknesses of about 300 nm at the wafer centre. The actual thickness variation (wedges) would depend on the elements being used, i.e. atomic volumes, adjusted for the measured composition at each point. The wedges mostly compensate each other, so the thickness variation is from somewhat less, to a lot less than the single wedge thickness variation (which was measured as approximately 40% using various targets). The atomic volumes of the Ta ($10.9 \text{ cm}^3 \text{ mol}^{-1}$) and Nb ($10.8 \text{ cm}^3 \text{ mol}^{-1}$) are pretty similar, so one can reasonably assume that the wedges essentially compensate (in a direct line). Additionally, pure Ta and pure Nb thin films were successively deposited on oxidised Si wafers in the same conditions from single targets for serving as reference samples. After the co-deposition of the Nb-Ta compositional spread, energy dispersive X-ray spectroscopy (EDX) was used for mapping the element concentrations across each wafer. The concentration gradient direction is dictated by the co-deposition geometry and the position of the targets. A precise measuring of the concentration gradient allowed an accurate identification of Nb-Ta alloys along the combinatorial library. More details about combinatorial libraries preparation can be found elsewhere [19].

2.2. Microelectrochemical setup

A scanning droplet cell microscope (SDCM) was used for the high throughput growth and characterization of anodic oxides of individual alloys on the surface of the Nb-Ta combinatorial library. The cell was built in an acrylic block having a three-electrode configuration [20]. Using a thermal puller (PC-10, Narishige), a borosilicate glass capillary with a 2.5 mm outer diameter was pulled and a tip with a diameter of $200 \mu\text{m}$ was obtained using a micro-grinder (EG-400, Narishige). This capillary was used as the outer body of the cell. A micro-reference electrode capillary with a $100 \mu\text{m}$ tip diameter ($\mu\text{-AuHg/Hg}_2(\text{CH}_3\text{COO})_2/\text{NaCH}_3\text{COO}$) was used for the SDCM measurements [21]. The counter electrode was fabricated using a thin Au band which was wrapped around the reference electrode. The reference and counter electrodes were inserted together into the main capillary body. More details regarding the reference electrode and cell fabrication can be found elsewhere [22]. For a precise definition of the wetted area on the investigated surface (working electrode) a silicone gasket was fabricated at the tip of the cell by immersing it into liquid silicone followed by drying in flowing nitrogen. A high reproducibility of this surface was ensured by pressing the tip against the investigated surface with a predefined force (3 mN) for producing only an elastic deformation of the sealing. In the same time, the electrolyte-air contact was avoided during the electrochemical investigations and the wetted area on the surface of the compositional spread had a very high reproducibility, with errors smaller than 1%, as previously demonstrated on pure Hf films [23].

2.3. Hardware description and measurement details

Since the investigated metallic alloys have a spread in composition along the surface of the samples (wafers), an automated, high-throughput measurement approach was necessary. Thus, the SDCM used for the electrochemical investigations on the Nb-Ta thin film library was fully computer controlled. Self-made control and data acquisition programs written with LabView software were used for controlling all the components of the SDCM system:

- a video camera providing live imaging of the sample, for definition of the scanning points/areas
- an XYZ translation stage, for high precision positioning of the SDCM tip on the sample surface
- a force sensor (KD45 2 N, ME-Messsysteme) combined with a lock-in amplifier (EG&G 7265), for the automated control of the applied force while pressing the SDCM tip against the sample
- a micro-syringe pump (Micro 4, World Precision Instruments), combined with a $100 \mu\text{l}$ syringe, for dosing the electrolyte from the cell in order to wet the investigated spot

The electrical contact to the metallic surface was achieved using a W needle in hard contact with the sample surface. More details about the automation of the SDCM and its software can be found elsewhere [22,23].

Scanning electron microscopy (SEM) was used for the characterisation of the Nb-Ta composition spread microstructure. Grazing incidence X-ray diffraction (GIXRD) performed at 1° , was used for the local crystallographic investigation of the thin film alloys. The irradiated spot had an elliptical shape ($3 \text{ mm} \times 7 \text{ mm}$), the small diameter of 3 mm being oriented parallel to the compositional gradient. Due to the compositional resolution measured by EDX ($0.3 \text{ at.}\% \text{ mm}^{-1}$) this means that individual alloys can be investigated by XRD with a resolution of 1 at.%. The X-ray diffraction results were correlated with the composition map obtained by EDX in order to obtain a complete description of the Nb-Ta combinatorial library before the electrochemical treatment. The

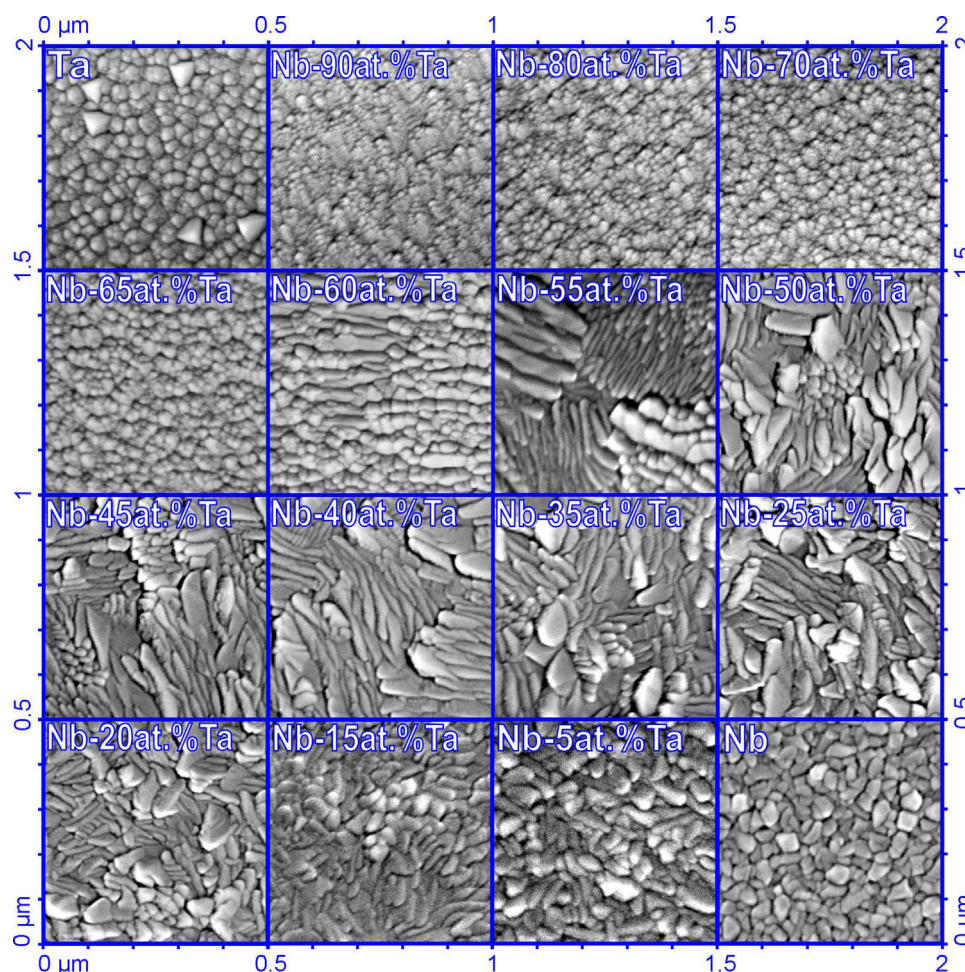


Fig. 1. SEM images of the Nb-Ta combinatorial library at different concentrations together with the pure Ta and Nb as references.

library surface was locally anodized in an acetate buffer electrolyte (pH 6.0) prepared from p.a. chemicals and de-ionized water using a potentiostat (Solartron Schlumberger 1287). The Nb-Ta composition spread was scanned in steps of 1 at.% composition difference and small oxide spots were locally grown. The anodizations were carried out potentiodynamically at a potential scan rate of $100 \text{ mV} \cdot \text{s}^{-1}$. Cyclic voltammograms (CVs) having the upper potential limit between 1 V and 10 V were sequentially recorded in 1 V steps for each investigated composition. Before each cyclic voltammogram, the impedance of the already formed oxide layer was measured at high (1 kHz) and low (0.1 Hz) frequency using a frequency response analyzer (S5720 C, NF Electronic Instruments) with a 10 mV AC voltage perturbation in order to determine the dielectric constant and electric resistivity of the anodic oxides in-situ during their growth. Mott-Schottky analysis was performed across the composition spread by measuring the capacitance of a 3 V potentiostatically grown oxide spot at different DC biases. X-ray photoelectron spectroscopy (XPS) was used for the in-depth chemical analysis of the Nb-Ta library at different compositions. Sputter depth profiles were recorded using 2 keV Ar^+ sputtering.

3. Results and Discussion

3.1. Microstructure of Nb-Ta thin films

The microstructure of the Nb-Ta combinatorial library was investigated using SEM and the results are shown in Fig. 1. Cross-section observations at selected compositions (not shown here)

have confirmed the presence of a columnar structure across the entire Nb-Ta compositional spread, typical for thin film formation by sputtering. Images of the alloy surfaces are presented in squares of $500 \text{ nm} \times 500 \text{ nm}$ for various compositions starting from the surface of pure Ta and ending with pure Nb films (shown as references). The surface of pure Ta films shows two different types of grains. The majority of the grains are round shaped, approximately 50 nm in diameter and form a compact structure. A smaller number of pyramidal grains can also be observed on the surface of Ta films. Small amounts of Nb start to disturb this structure, the pyramidal grains being totally suppressed by 90 at.% Ta. At this concentration, finer grains with an approximate diameter of 20 nm start to appear preferentially clustered at the boundaries of bigger domains. A very similar evolution was previously observed in Ta-Ti and Hf-Ta thin film binary libraries, where small amounts of Ti or Hf had the same effect on the surface microstructure [24,25]. At around 70 at.% Ta, an almost-uniform grain size can be observed and the evolution of the microstructure leads to formation of an in-plane columnar structure which is visible for Nb-60 at.%Ta. Columns with the same width are fast grouping in larger domains with clearly visible domain boundaries at Nb-55 at.%Ta. Several grain sizes can be identified at this point, the equivalent diameter of the columns ranging between 20 and 100 nm. With the increase of the Nb concentration with another 5 at.%, the newly formed domains appear to interact strongly with each other having as a result the formation of less defined domain boundaries. This microstructure appears to be stable until very high Nb concentrations are reached. The grains evolve and in the same time the columnar structure changes and

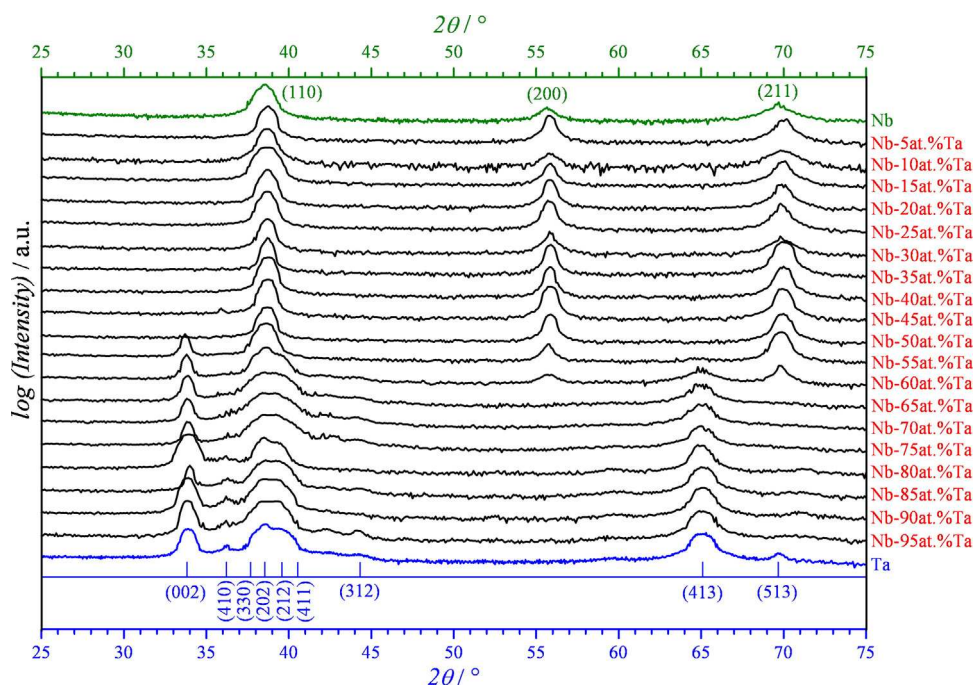


Fig. 2. GIXRD patterns measured at various concentrations of the Nb-Ta library.

only one type of grains can be observed at Nb-5 at.%Ta, resembling the microstructure of pure Nb which shows a relatively compact microstructure with grain sizes below 100 nm.

The crystallographic properties of the Nb-Ta binary library, investigated using X-ray diffraction are summarized in Fig. 2 together with the spectra recorded for pure Ta and Nb films. For all films, polycrystalline structures could be identified. Pure Ta films show a tetragonal symmetry while pure Nb films have a cubic structure. If the peak intensities of the pure Ta films are matching those of bulk polycrystalline Ta, pure Nb thin films show a weaker (110) peak. This decrease of intensity may be attributed to a suppression of the main (110) orientation observed in bulk cubic Nb and may be interpreted as a preferential growth of (110) plane parallel to the growth direction. The crystallographic evolution of the Nb-Ta binary library can be correlated with the microstructure evolution presented in Fig. 1. Starting from pure Ta and increasing the amount of Nb in the alloys, no crystallographic changes can be detected up to Nb-65 at.%Ta. This composition range, corresponding to the fine grained microstructure from Fig. 1, shows only thin film alloys with tetragonal structure. The columnar microstructure formation at Nb-60 at.%Ta coincides with the incipient formation of a cubic phase in the alloys. Even though the positions of the (513) tetragonal peak and the (211) cubic peak are almost the same, the sudden appearance of this peak for 60 at.% Ta together with the presence of a clear (200) cubic peak strongly suggests a cubic phase for this alloy. In the same time, the presence of the broad peak centred at 38.5° which contains several tetragonal peaks indicates that the tetragonal structure still exists, Ta-40 at.%Nb representing a transition step from tetragonal to cubic structures. This conclusion is further supported by the clear establishment of the cubic structure at Ta-50 at.%Nb when the (002) tetragonal peak eventually disappears. The cubic structure remains stable while increasing the Nb concentrations, until the pure Nb structure is reached. A similar crystallographic threshold was previously found when the tetragonal structure of Ta was perturbed by the presence of Ti in a Ta-Ti binary library. However, in that case no coexistence of both tetragonal and cubic symmetries was found for a single alloy (during a similar XRD scanning with 5 at.% resolution), even though Ta, Ti and Nb all have identical atomic radii (145 pm) [24]. The

role of cubic phase stabilizer of Nb was also evidenced in mixtures with Ti during the analysis of a Nb-Ti thin film library, when lower amounts of Nb (<25 at.%) were already sufficient for a complete β phase formation for Ti [26].

3.2. Potentiodynamic oxide formation and characterization

In order to investigate the particularities of anodic oxide formation on Nb-Ta thin film alloys, both potentiodynamic and potentiostatic experiments were locally performed using the SDCM. Selected cyclic voltammograms recorded during anodisations of Nb-Ta thin film alloys are presented in Fig. 3. The step-wise anodisations from 1 to 10 V, with a scan rate of 100 mV s^{-1} can be observed for a few representative compositions of the Nb-Ta library. A typical valve metal behaviour characterized by current suppression when the potential starts to decrease in the backward scan of each CV loop is observed. Up to 5 V, the overshoot characteristic to low oxide formation potentials is present in all cases of

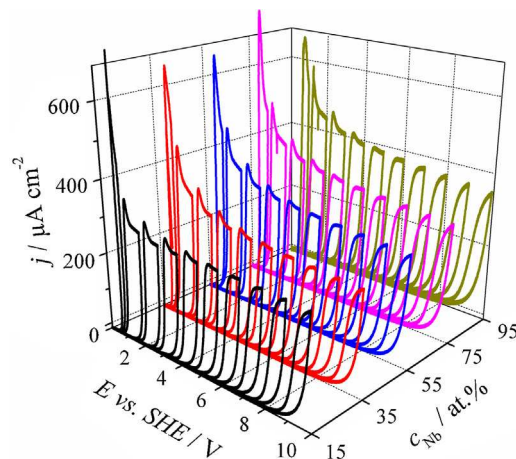


Fig. 3. Cyclic voltammograms recorded during the potentiodynamic oxide growth on Nb-Ta alloys at different concentrations.

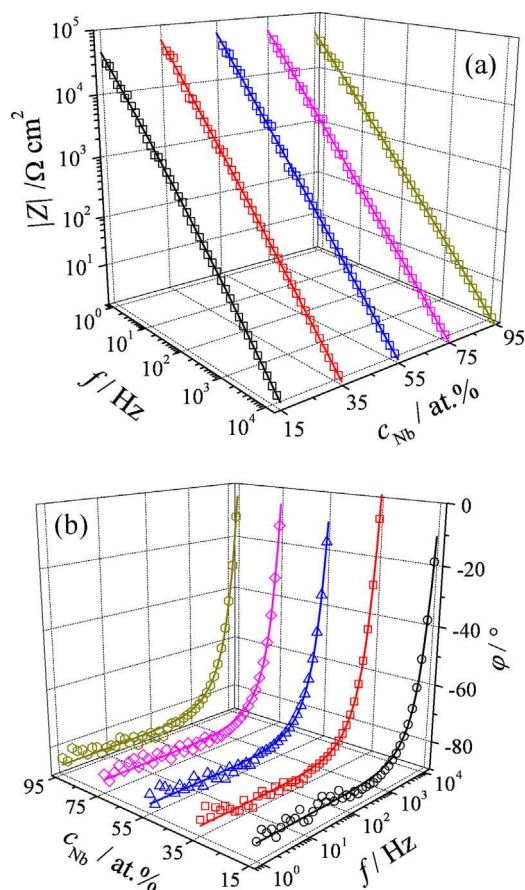


Fig. 4. Electrochemical impedance spectroscopy of anodic oxides grown potentiostatically at 3 V on the Nb-Ta composition spread for different concentrations. Impedance modulus (a) and phase (b) frequency dependence.

the first CV steps. After exceeding the former oxidation potential, a steep increase in current is observed until reaching a plateau current density which is a direct consequence of the stoichiometric oxide growth without side reactions [27]. For each sample, a different current density plateau corresponding to a constant rate of oxide thickness increase can be observed. The value of this plateau is proportional to a specific oxide formation factor (expressed in nm V^{-1}) and the inverse of the rate of potential increase through a proportionality constant which depends on oxide density, molar mass and number of exchanged electrons per formula unit. For calculating the oxide density of the Nb-Ta alloys, a mixed matter model was used that assumes a linear distribution between the densities of the pure Ta_2O_5 and Nb_2O_5 (8.10 and 4.36 g cm^{-3} , respectively). The oxide formation factor which represents the inverse of the electric field driving the ion hopping mechanism of oxide formation is useful for direct determination of the oxide thickness for certain anodisation potentials [28].

Using the SDCM, full impedance spectra of anodic oxides grown potentiostatically at 3 V were recorded at different concentrations in the Nb-Ta library for assessing the general behaviour before the single frequency impedance measurements could be conducted. In Fig. 4 these results are shown for a few representative Nb concentrations. The impedance (a) and the phase shift (b) are plotted as a function of frequency for an applied bias of 0 V (SHE). All investigated oxides showed a typical -1 slope in the double-logarithmic plot of the impedance. Starting from high frequencies, all phase shifts decrease rapidly and values close to -90° are already detected at 1 kHz suggesting a pure capacitive behaviour. This leads to concluding that 1 kHz is a suitable value for single frequency

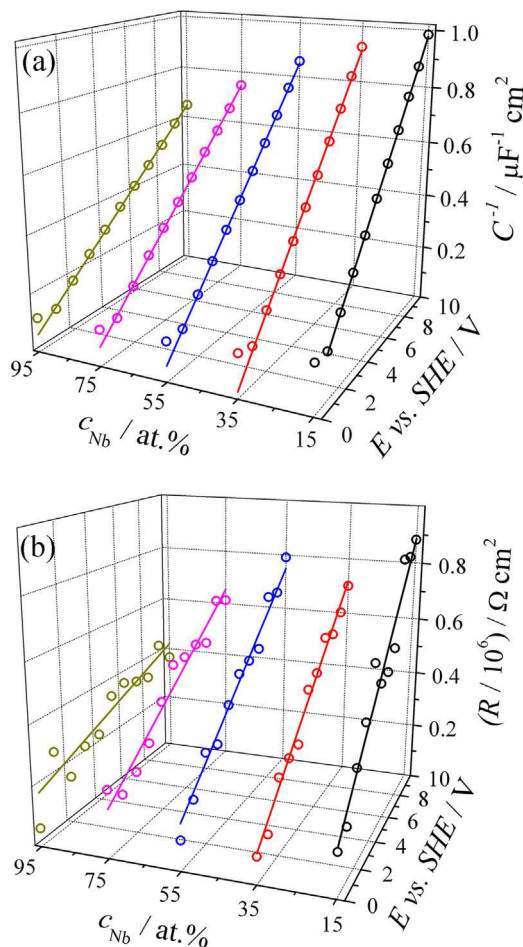


Fig. 5. (a) Inverse capacitance and (b) electric resistance of anodic oxides measured after each 1 V step in the anodization potential for various compositions of the Nb-Ta thin film alloys.

measurements of impedance during the automatic scanning of the Nb-Ta composition spread for capacitive characterisation of the anodic oxides as a function of parent metals composition. A low frequency such as 0.1 Hz can be used for the measurement of oxides resistances. As soon as this frequency is approached, the noise level considerably increases (not shown in Fig. 4) but overall the phase shift approaches -75° indicating the transition toward the resistive behaviour of the anodic oxides. Such full spectra EIS were not done at every investigated Nb-Ta composition due to the long acquisition time necessary for measurements with 1 at.% resolution. The impedance data shown in Fig. 4 suggest that a simple RC parallel circuit characterising the oxide, in series with a small electrolyte resistance (approximately 10Ω), can be used for describing the anodic oxides. This equivalent circuit was also used previously for other valve metal alloys containing Ta and Nb [24–26].

The automated operation mode of the SDCM was used for in-situ single frequency impedance measurements of anodic oxides after each 1 V anodisation step. In Fig. 5 are presented the inverse capacitances (a) and the resistances (b) of anodic oxides grown on the surface of the Nb-Ta binary thin film library as a function of anodisation potentials. The values of the inverse capacitance show a good linear dependence on the potential, while the values of the resistance show a more dispersed distribution. This is mainly due to the very low currents (10^{-8} A) measured during the low frequency investigations which normally have low signal-to-noise ratio. Due to the fact that the anodisation potential is directly related to the oxide thickness through the oxide formation factor, the slopes of

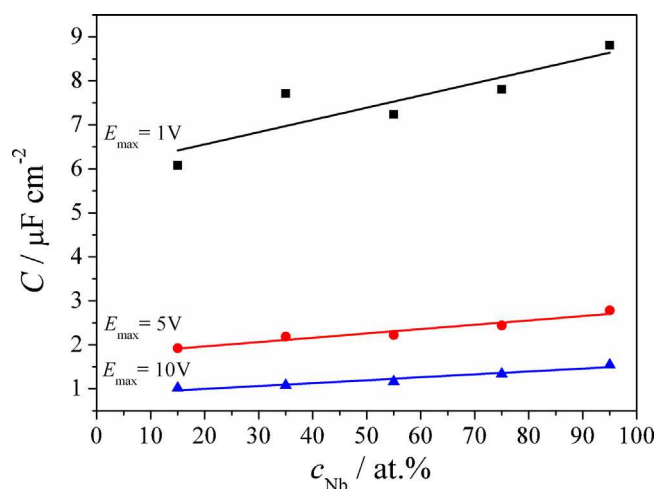


Fig. 6. Mixed Nb-Ta anodic oxide capacitance dependence on the Nb content along the Nb-Ta compositional spread. Three different anodization potentials (1 V, 5 V and 10 V) are indicated in the graph.

the curves presented in Fig. 5 (a) and (b) will allow a direct calculation of the dielectric constants and electrical resistivities of the anodic oxides, respectively. The area normalized capacitance values of the anodic oxides grown along the Nb-Ta compositional spread are also mapped along the compositional gradient. In Fig. 6 the oxide capacitance directly obtained from fitting the EIS data is plotted as a function of Nb content for three different anodisation potentials: 1 V, 5 V and 10 V vs. SHE. In all cases, an almost linear behaviour can be identified. Also, the positive slopes of these curves indicate that the dielectric constant of the mixed Nb-Ta anodic oxide increases faster with the Nb content than the oxide thickness. This conclusion is based on both direct proportionality between the anodisation potential and oxide thickness and inverse proportionality between the oxide capacitance and its thickness. A similar trend was previously evidenced also in thicker Nb-Ta oxides [15].

In Fig. 7 (a) the dielectric constants of the mixed Nb-Ta anodic oxides are plotted for the entire binary library with a resolution of 1 at.%. Starting from low values ranging between 20 and 25 for low Nb concentrations, the electric permittivity of the anodic oxides gradually increases until a maximum value of 53 is measured on pure Nb₂O₅. These findings confirm and complete the values previously reported when analysing anodic oxides grown on discrete Nb-Ta thin film compositions [14,15]. Since multiple peaks may be found in this type of dependence, a multi-peak Lorentzian type distribution function was used for fitting the experimental data in order to observe the trends of the changes due to composition differences between the alloys. In the same graph the oxide formation factor k is also plotted as a function of the parent metals concentrations. Starting from the k value of 1.8 nm V⁻¹ measured on pure Ta, the k factor first decreases to approximately 1.6 nm V⁻¹ for the Nb-80 at.%Ta and then gradually increases with the Nb concentration until a value of 2.6 nm V⁻¹ is reached on pure Nb. The appearances of both curves are similar and the tendencies of increase or decrease are identical and happen at the same compositions. The smooth, almost linear increase of the oxide formation factor in the transitional composition zone from the tetragonal to cubic structure in the Nb-Ta library (Nb-65 at.%Ta to Nb-50 at.%Ta, Fig. 2) suggests at a first glance a smooth change to the cubic phase due to increasing amounts of Nb. The coexistence of both phases (observed in Fig. 2 for 60 and 55 at.%Ta) does not result in any remarkable behaviour of the oxide formation factor and dielectric constant along the compositional gradient. The values are naturally changing between the extreme values measured on pure Ta and pure Nb thin films.

In part (b) of Fig. 7 one can observe the dependence of the electrical resistivity of the anodic oxides on the composition of the Nb-Ta thin film binary library. The mapping of the electrical resistivity has the same compositional resolution of 1 at.% as the dielectric constant mapping. Compared with the data points shown in the part (a) of Fig. 7, the resistivity mapping shows a slightly higher scattering due to the low current measurements necessary for impedance spectroscopy at low frequencies (0.1 Hz). Starting from pure Ta, a multi-peak Lorentzian fit shows first a small increase in oxides resistivities with a maximum positioned at approximately Nb-85 at.%Ta. This coincides with the small decrease of both oxide formation factor and dielectric constant shown in the mappings from Fig. 7 (a). Increasing the Nb content in the Nb-Ta library, the anodic oxide electrical resistivities start to decrease until approximately 2.5 10¹¹ Ω cm can be measured for 65 at.% Nb. When increasing the Nb concentration even more, this value shows a small fluctuation with a peak at around 80 at.% Nb. During the entire mapping of the electrical resistivity, the experimental curve had an approximately opposite evolution as compared with both oxide formation factor and dielectric constant mappings. This behaviour was not always found in Ta alloys, being reported for Hf-Ta but not found in Ta-Ti thin film combinatorial libraries [24,25].

3.3. Semiconducting properties analysis

Ta₂O₅ is a good insulator with a band gap of 5.1 eV while Nb₂O₅ shows semiconducting properties due to a band gap of only 3.4 eV [29]. During the anodic oxidation of the Nb-Ta parent metals, a mixed oxide formed from both Ta₂O₅ and Nb₂O₅ is to be expected. The semiconducting properties of thin Nb-Ta anodic oxides grown potentiostatically at 3 V were assessed by using a Mott-Schottky analysis in a second automated SDCM scan of the entire library following the step-wise potentiodynamical anodization scan. For each investigated Nb-Ta composition, the anodic oxide was biased at various potentials without exceeding the maximum oxide formation potential, and the capacitance of the formed space charge layer (C_{SC}) was determined. The surface of the Nb-Ta compositional spread was scanned and in Fig. 8 the curves describing the relationship between the inverse squared capacitance and the applied bias for various concentrations of the parent metals are presented with a resolution of 5 at.%. This relationship is dictated by the famous Mott-Schottky equation:

$$C^{-2} = C_{SC}^{-2} = 2(E - E_{FB} - k_{BT}/q)/(qN_D\epsilon\epsilon_0)$$

where $E - E_{FB}$ represents the potential difference across the oxide film with E_{FB} being the flat band potential, q is the elementary charge, k_{BT}/q is the potential variation due to thermal effects (25.8 mV at 300 K), N_D is the density of the carriers (donors) ϵ is the dielectric constant (relative permittivity number) of the oxide and ϵ_0 is the vacuum permittivity. For all Nb-Ta alloys, indications of an n type semiconductor were found due to the positive slopes of the linear parts of the Mott-Schottky plots from Fig. 8. The slopes of the Mott-Schottky plot linear fits and their intercepts (not shown here) can directly be used for calculating the flat band potentials and donor concentrations of the anodic oxides on Nb-Ta library, using the dielectric constants mapping from Fig. 7. The results are summarised in Fig. 9 with a resolution of 5 at.% together with the values previously found for the pure oxides [29]. Starting from a cathodic value slightly below -1 V for the anodic oxide on Nb-95 at.%Ta, the flat band potentials are constantly increasing with the increase of Nb amount in the Nb-Ta combinatorial library until an anodic value of 0.5 V is reached for 95 at.% Nb. This almost linear increase is another indication that the properties of both parent metal alloys and their anodic oxides are smoothly changing as a function of composition. Having a low value just above 2·10¹⁹ cm⁻³

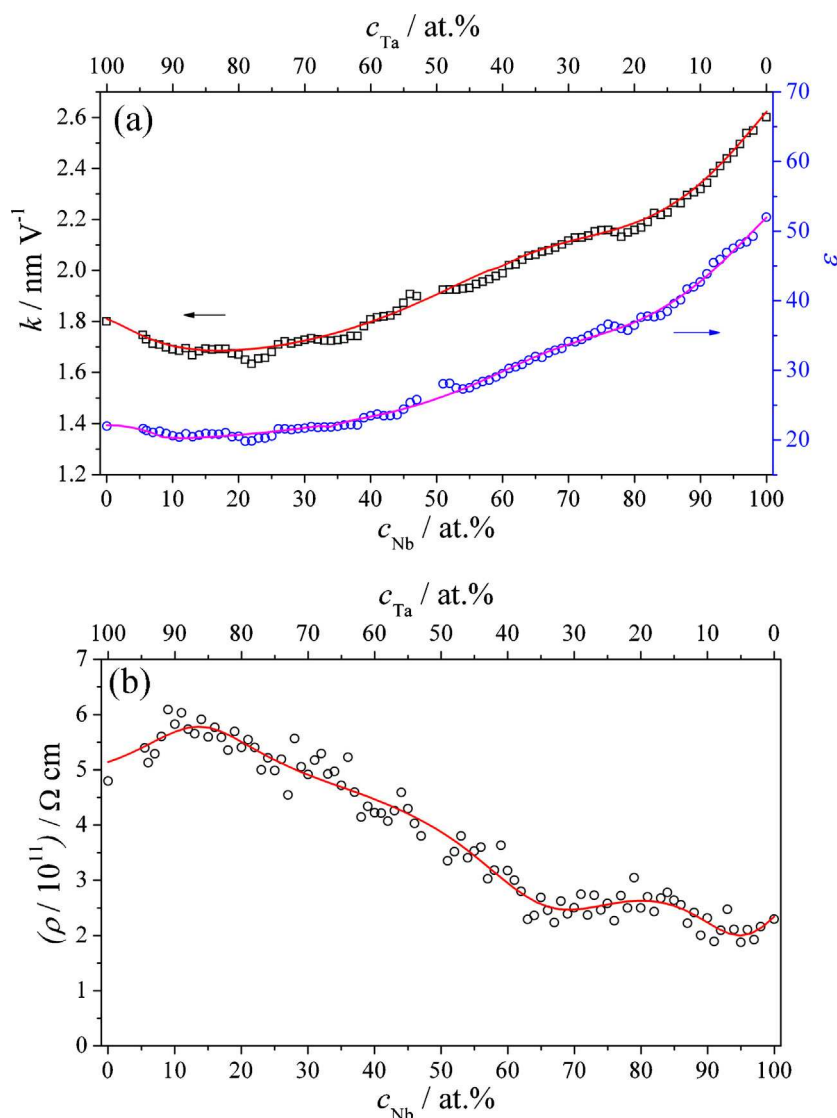


Fig. 7. (a) Oxide formation factors, dielectric constants and (b) electrical resistivities for the anodic oxides grown on the Nb-Ta combinatorial library with a maximum applied potential of 10 V vs SHE.

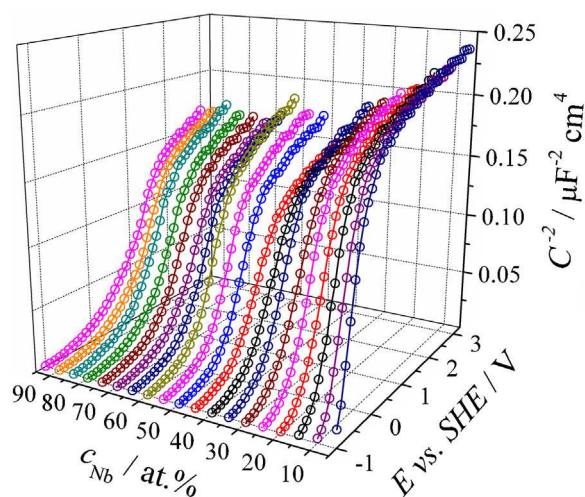


Fig. 8. Mott-Schottky plots for the anodic oxides potentiostatically grown at 3 V vs. SHE on the Nb-Ta combinatorial library at different concentrations.

at low Nb concentrations, the oxide donor densities presented also in Fig. 9 show a maximum with a value of almost $6 \cdot 10^{19} \text{ cm}^{-3}$. This peak is centred in the compositional transition region between the tetragonal and cubic structures (see Fig. 2) showing that the coexistence of both phases in the parent metals have also an effect on the semiconducting properties of the anodic oxides. Increasing the Nb content further, the donor concentration almost stabilizes around $4 \cdot 10^{19} \text{ cm}^{-3}$ and later falls below this value for Nb-5 at.%Ta.

In all Nb-Ta anodic oxide properties presented so far, a rather smooth change along the compositional gradient can be observed. Oxide-specific parameters (e.g. formation factor, dielectric constant or electrical resistivity shown in Fig. 7) as well as semiconducting properties (see Fig. 9) do not show any abrupt changes along the compositional gradient as would be suggested by the sudden crystallographic change observable in the GIXRD investigations from Fig. 2. This may lead to concluding that the amorphous nature of the Nb-Ta oxides is probably responsible for this fact. A compositional dependence rather than a strong crystallographic influence is observed throughout the mapping of anodic oxide properties along the Nb-Ta thin film combinatorial library.

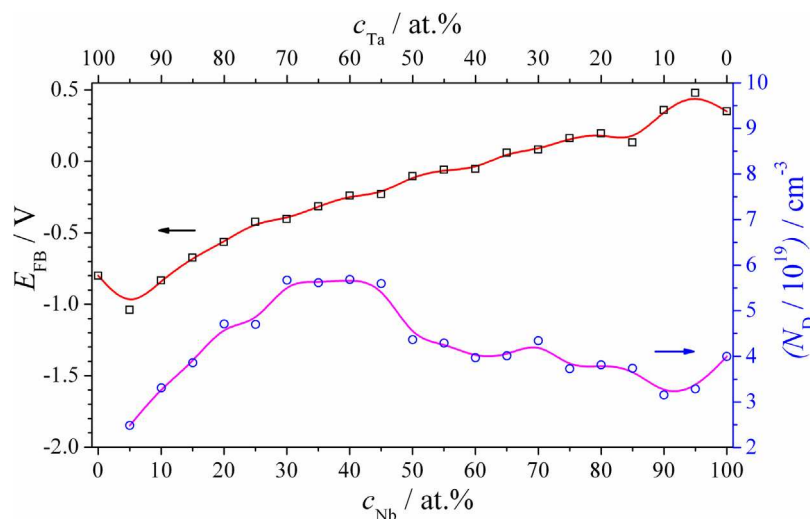


Fig. 9. Flat band potential and donor concentration of anodic oxides potentiostatically grown at 3 V vs. SHE on the Nb-Ta library as a function of concentrations.

3.4. Surface analytical investigations

For a better understanding of the anodic oxidation on the surface of the Nb-Ta thin film composition spread, XPS depth profiling was used. In Fig. 10 the spectra for Ta (left side) and Nb (right side) for three different concentrations (75, 45 and 15 at.% Ta) are presented which are distributed along the investigated composition spread. The depth scale (given in the right part of the graphs in nm) refers to the calibrated equivalent sputtering depth in SiO₂. Similar depth profiles measured on potentiodynamically anodised pure Ta and pure Nb thin films (not shown here) suggested that the SiO₂ depth scale is overestimated when used for the anodised Nb-Ta alloys. This is due to the inconsistencies observed between the detected depth (on the SiO₂ scale) at which the metallic peaks start appearing and the measured oxide thickness from the electrochemical anodization data. Since the oxide sputter rates can not be precisely known due to the concentration gradient in the Nb-Ta combinatorial library, the SiO₂ depth scale was preferred here as an estimative depth scale.

For all presented cases, both Ta and Nb oxides can be identified on the surface of the thin film library which indicates that the oxides are mixing during the anodisation process, most likely in a competition process for combining with oxygen ions. This suggests the formation of a mixed Nb-Ta anodic oxide, where the amount of each oxidised species will be influenced by both, metallic parent concentrations and ionic state of the individual oxides. The intensities of the XPS peaks are varying with the parent metals concentrations and with the depths. In the left column of Fig. 9, the in-depth behaviour of the Ta oxide can be followed along the compositional spread. For low amounts of Nb, metallic Ta can be already found together with oxidised ions at depths of about 10 nm (Nb-75 at.%Ta). When the amount of Nb in the library is increased, this depth also increases to a value of about 26 nm for Nb-15 at.%Ta. The right column of Fig. 9 shows the complementary behaviour of Nb oxide for the same previously selected compositions in the Nb-Ta combinatorial library. Increasing the sputtering depths, a clear shift to lower energies of the oxidised Nb peaks can be observed. Since the position of the Nb 3d_{5/2} peak at the highest depth of 30 nm does not match the value for the metallic Nb (202 eV), it can be concluded that the shift can be attributed solely to the oxide reduction due to energy transfer between the incident Ar and Nb ions [30]. This shift was previously found to be more accentuated in Ti-Nb alloys [26].

A quantitative evaluation of the XPS spectra recorded on the library surface (before the Ar sputtering) was done by integrating the XPS peaks and the results are summarised in Table 1. The quantitative evaluation shows that the ratios between the oxidised species of Ta and Nb in the mixed anodic oxide are changing as compared with the ratios between the metallic parents along the entire library. These ratios are presented in Table 1 together with the concentration deviations (in percent) from the parent metal compositions. Even though the surface composition of the anodic oxides deviates from the composition of the metallic alloys, no clear trend can be observed. Previous in-depth investigations of thicker Nb-Ta anodic oxides (anodized at 80 V) indicated that regardless of the alloy compositions, the migration rate of Ta ions is about 0.75 that of Nb ions. This produced a segregated anodic oxide structure with a Nb₂O₅ top-most outer layer [15]. However, on the top-most anodic oxide surface layer, the situation is slightly different in the present study due to kinetic effects directly related to the much smaller thickness of the oxides analysed here. High concentrations of Ta in the metallic phase lead to the presence of more Nb in the oxidised phase (e.g. Nb-90 at.%Ta, Nb-75 at.%Ta) whereas high concentrations of Nb in the metallic phase had as a result higher amounts of Ta being found in the oxidised phase (e.g. Nb-15 at.%Ta, Nb-5 at.%Ta). In the middle of the compositional spread, the compositional deviation is randomly distributed with values oscillating with a few percent around 0 for both Ta and Nb. The absence of a clear trend in the compositional deviations of the oxides as compared with their parent metals can be attributed to the identical transport numbers of Ta and Nb (0.24) [31,32]. Both Ta and Nb ions have equal probabilities for finding oxygen in the process of oxide formation and the only factor which can influence this is the Nb:Ta ratio present in the parent metals. It is expected that the predominant atomic

Table 1

Metal concentration ratios for the parent metal alloys (Me), anodic oxides (Ox) and their individual variations with respect to the metal concentrations ($\Delta^{Me:Ox}$).

Nb _{Me} :Ta _{Me} (at.%)	Nb _{Ox} :Ta _{Ox} (at.%)	$\Delta^{Me:Ox}$ Nb (%)	$\Delta^{Me:Ox}$ Ta (%)
10: 90	13.7: 86.3	+37.0	-4.1
25: 75	26.1: 73.9	+4.4	-1.5
40: 60	38.6: 61.4	-3.5	+2.3
55: 45	61.0: 39.0	+10.9	-13.3
85: 15	78.4: 21.6	-7.8	+44.0
95: 5	92.0: 8.0	-3.2	+60.0

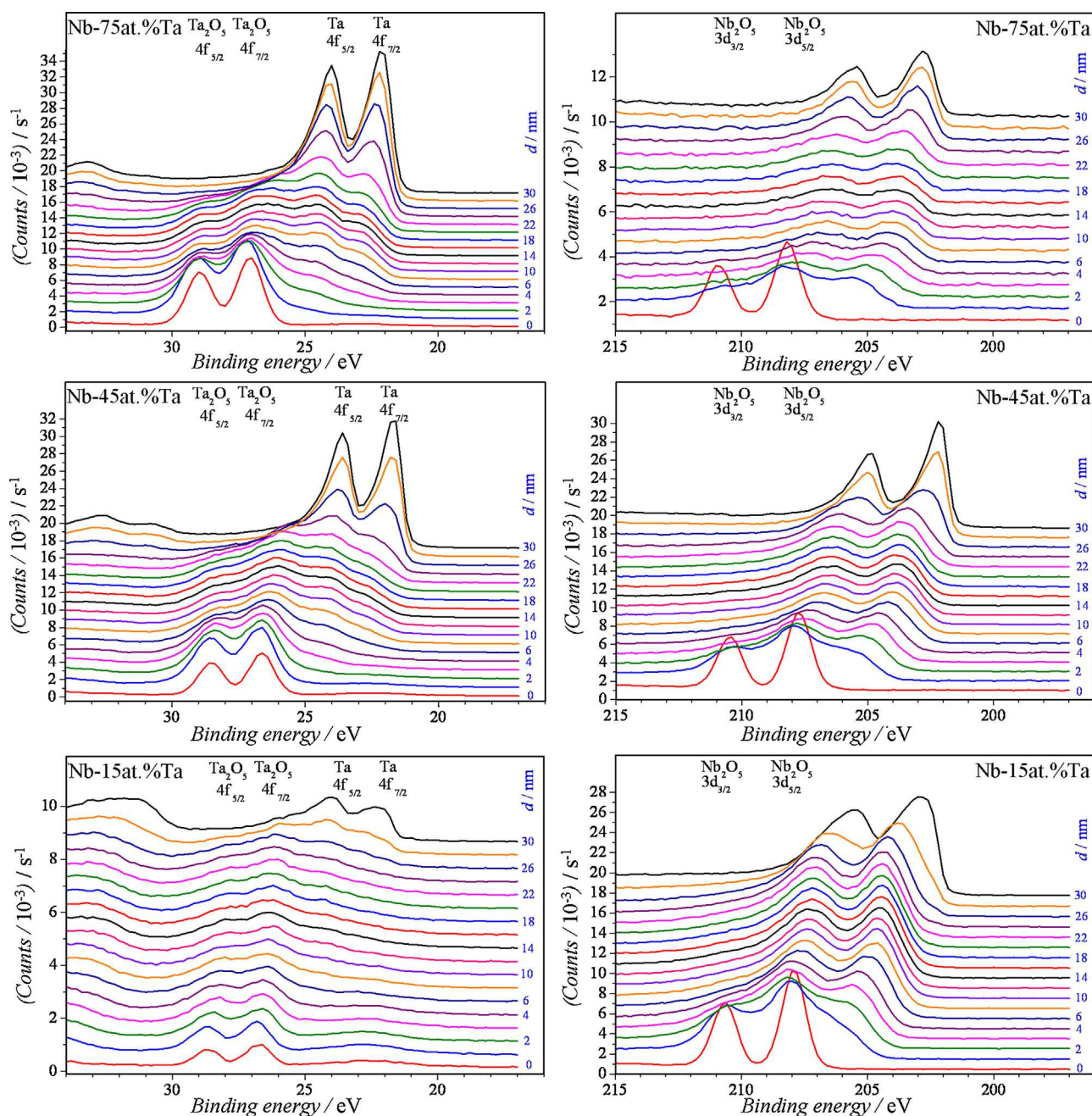


Fig. 10. XPS depth profiling spectra of the anodic oxides grown on the Nb-Ta combinatorial library at different compositions with a maximum applied potential of 10 V vs. SHE.

species would have a higher probability of forming anodic oxide. Since the transport number dictates that both Ta and Nb oxides are growing 3 times faster at the oxide/metal interface as compared to the electrolyte/oxide interface, the minority atomic species would be found more at the electrolyte/oxide interface (which represents the surface of the mixed oxide). This would explain why more Nb ions can be found on the surface of the anodic oxide when the Ta amount in the metallic alloys is higher (and vice versa).

4. Conclusions

A wide spread Nb-Ta thin film combinatorial library (Nb-5 at.%Ta to Nb-94 at.%Ta) deposited using a co-sputtering technique was investigated. The microstructure and crystallographic properties of the Nb-Ta thin films were locally mapped along the compositional

gradient using SEM and XRD, respectively. Starting from pure Ta, a relevant microstructure change was observed at Nb-60 at.%Ta when an in-plane columnar structure became visible immediately followed by formation of domains. This correlates to the crystallography of the Nb-Ta thin film alloys since at this compositional threshold the transition from tetragonal to cubic symmetry is evidenced by a mixed tetragonal-cubic phase. The anodic oxide growth on the surface of the Nb-Ta thin film library was locally studied using a scanning droplet cell microscope. Oxide formation factors and electric properties of the mixed anodic oxides were mapped along the entire compositional spread using cyclic voltammetry and electrochemical impedance spectroscopy, respectively. Due to the semiconducting character of Nb oxide, Mott-Schottky analysis was employed for mapping the semiconducting properties of the mixed Nb-Ta anodic oxides. Type-n semiconducting

behaviour was evidenced. Qualitative and quantitative chemical analysis of the anodic oxides was achieved via XPS depth profiling. The chemical composition of the surface anodic oxides was compared to the composition of the parent metal alloys and no clear trend could be identified regarding their mismatch. This was attributed to the identical ionic transport numbers of Ta and Nb.

Acknowledgements

The financial support by the Austrian Federal Ministry of Economy, Family and Youth and the National Foundation for Research, Technology and Development is gratefully acknowledged.

References

- [1] M. Pourbaix, *Atlas of electrochemical equilibria in aqueous solutions*, National association of corrosion engineers, Houston, 1974.
- [2] Gmelin Handbook of inorganic and organometallic chemistry, Vol. Tantalum–Ta, Springer, New York, 1997.
- [3] A.W. Hassel, D. Dising, Breakdown of ultrathin anodic valve metal oxide films in metal-insulator-metal-contacts compared with metal-insulator-electrolyte contacts, *Thin Solid Films* 414 (2002) 296.
- [4] M. Ishizuka, E. Tsuji, Y. Aoki, H. Habazaki, Formation and dielectric properties of anodic films formed on Ta–W alloys at various formation voltages, *Electrochemistry* 81 (2013) 840.
- [5] M.G. Golkovski, I.A. Bataev, A.A. Bataev, A.A. Ruktuev, T.V. Zhuravina, N.K. Kusanov, R.A. Salimov, V.A. Bataev, Atmospheric electron-beam surface alloying of titanium with tantalum, *Mater. Sci. Eng. A* 578 (2013) 310.
- [6] X.H. Chen, P.Z. Zhang, D.B. Wei, J. Huang, W. Xuan, Surface modification of pure titanium by plasma tantalumising, *Surf. Eng.* 29 (2013) 228.
- [7] M. Valant, D. Suvorov, New high-permittivity $\text{AgNb}_{1-x}\text{Ta}_x\text{O}_3$ microwave ceramics: Part II, Dielectric characteristics, *J. Am. Ceram. Soc.* 82 (1999) 88.
- [8] M. Valant, A.K. Axelsson, N. Alford, Review of $\text{Ag}(\text{Nb}, \text{Ta})\text{O}-3$ as a functional material, *J. Eur. Ceram. Soc.* 27 (2007) 2549.
- [9] M. Wenderoth, S. Vorberg, B. Fischer, Y. Yamabe-Mitarai, H. Harada, U. Glatzel, R. Völkl, Influence of Nb, Ta and Ti on microstructure and high-temperature strength of precipitation-hardened Pt-base alloys, *Mater. Sci. Eng. A* 483–484 (2008) 509.
- [10] E. Joanni, A.I. Mardare, C.C. Mardare, J.R.A. Fernandes, Simple method for crystallizing ceramic thin films using platinum bottom electrodes as resistive heating elements, *Jpn. J. Appl. Phys.* 2 (42) (2003) L863.
- [11] Y. Dai, J.H. Li, X.L. Che, B.X. Liu, Proposed long-range empirical potential to study the metallic glasses in the Ni–Nb–Ta system, *J. Phys. Chem. B* 113 (2009) 7282.
- [12] M.H. Lee, J.-H. Kim, J.S. Park, J.C. Kim, W.T. Kim, D.H. Kim, Fabrication of Ni–Nb–Ta metallic glass reinforced Al-based alloy matrix composites by infiltration casting process, *Scripta Mater.* 50 (2004) 1367.
- [13] A.I. Mardare, M. Kaltenbrunner, N.S. Sariciftci, S. Bauer, A.W. Hassel, Ultra-thin anodic alumina capacitor films for plastic electronics, *Phys. Status Solidi A* 209 (2012) 813.
- [14] F. Di Franco, G. Zampardi, M. Santamaria, F. Di Quarto, H. Habazaki, Characterization of the solid state properties of anodic oxides on magnetron sputtered Ta, Nb and Ta–Nb alloys, *J. Electrochem. Soc.* 159 (2012) C33.
- [15] S. Komiya, E. Tsuji, Y. Aoki, H. Habazaki, M. Santamaria, F. Di Quarto, P. Skeldon, G.E. Thompson, Growth and field crystallization of anodic films on Ta–Nb alloys, *J. Solid State Electrochem.* 16 (2012) 1595.
- [16] T.H. Muster, A. Trinch, T.A. Markley, D. Lau, P. Martin, A. Bradbury, A. Bendavid, S. Dligatch, A review of high throughput and combinatorial electrochemistry, *Electrochim. Acta* 56 (2011) 9679.
- [17] T.A. Aljohani, B.E. Hayden, A. Anastasopoulos, The high throughput electrochemical screening of the corrosion resistance of Ni–Cr thin film alloys, *Electrochim. Acta* 76 (2012) 389.
- [18] S.R. Taylor, The investigation of corrosion phenomena with high throughput methods: a review, *Corros. Rev.* 29 (2011) 135.
- [19] A. Ludwig, R. Zarnetta, S. Hamann, A. Savan, S. Thienhaus, Development of multifunctional thin films using high-throughput experimentation methods, *Int. J. Mater. Res.* 99 (2008) 1144.
- [20] A.W. Hassel, M.M. Lohrengel, The scanning droplet cell and its application to structured nanometer oxide films on aluminium, *Electrochim. Acta* 42 (1997) 3327.
- [21] K.A. Lill, A.W. Hassel, A combined mu-mercury reference electrode/Au counter-electrode system for microelectrochemical applications, *J. Sol. State Electrochem.* 10 (2006) 941.
- [22] A.I. Mardare, A.D. Wieck, A.W. Hassel, Microelectrochemical lithography: A method for direct writing of surface oxides, *Electrochim. Acta* 52 (2007) 7865.
- [23] A.I. Mardare, A.W. Hassel, Quantitative optical recognition of highly reproducible ultra thin oxide films in microelectrochemical anodisation, *Rev. Sci. Instr.* 80 (2009) 046106.
- [24] A.I. Mardare, A. Savan, A. Ludwig, A.D. Wieck, A.W. Hassel, A combinatorial passivation study of Ta–Ti alloys, *Corr. Sci.* 51 (2009) 1519.
- [25] A.I. Mardare, A. Ludwig, A. Savan, A.D. Wieck, A.W. Hassel, Combinatorial investigation of Hf–Ta thin films and their anodic oxides, *Electrochim. Acta* 55 (2010) 7884.
- [26] A.I. Mardare, A. Savan, A. Ludwig, A.D. Wieck, A.W. Hassel, High-throughput synthesis and characterization of anodic oxides on Nb–Ti alloys, *Electrochim. Acta* 54 (2009) 5973.
- [27] M.M. Lohrengel, Thin anodic oxide layers on aluminium and other valve metals—High-field regime, *Mater. Sci. Eng. R* 11 (1993) 243.
- [28] A.W. Hassel, M.M. Lohrengel, Preparation and properties of ultra thin anodic valve metal oxide films, *Mater. Sci. Forum* 185 (1995) 581.
- [29] J.W. Schultze, M.M. Lohrengel, Stability, reactivity and breakdown of passive films. Problems of recent and future research, *Electrochim. Acta* 45 (2000) 2499.
- [30] D. Briggs, M.P. Seah, *Practical surface analysis*, 1, J. Wiley & Sons, New York, 1993.
- [31] J.P.S. Pringle, Transport numbers of metal and oxygen during anodic-oxidation of Tantalum, *J. Electrochem. Soc.* 120 (1973) 398.
- [32] J.P.S. Pringle, The anodic-oxidation of superimposed metallic layers—Theory, *Electrochim. Acta* 25 (1980) 1423.